Real-Time Artefact Corrections For Quantitative MR Temperature Mapping

B. Denis de Senneville[1,2], P. Desbarats[1,2], B. Quesson[2], C. T. W. Moonen[1]
e-mail : {baudouin,desbarats,quesson,moonen}@rmsb.u-bordeaux2.fr

[1] RMSB / CNRS UMR 5536
Université Bordeaux 2
146, rue Léo Saignat
F-33076 Bordeaux, France

[2] Image Guided Therapy SA
2, allée du doyen George Brus
F-33600 Pessac, France

ABSTRACT

Apart from anatomical and physiological imaging, MRI can also be used to produce temperature maps. Our objective is to obtain such maps in real-time to monitor mini-invasive thermal therapies. The acquisition procedure of temperature MRI produces specific artefacts : noise generated by MRI, motion artefacts and geometric distortions. Here, numerical methods are described for attenuation of such artefacts. The methods are based on a physical description of the origin of such artefacts in MR temperature mapping.

Keywords

MRI, temperature maps, real-time image processing.

1. INTRODUCTION

In addition to its well established role as a diagnostic modality, Magnetic Resonance Imaging (MRI) is becoming increasingly important in therapeutic techniques. The quasi real-time acquisition of images allows control during the medical procedures.

Much interest have been recently focused on local hyperthermia using laser [Ger98], microwave [Sch95, Vit97], radiofrequency (RF) [Sam92, Wlo98], or focused ultrasound (FUS) [Cli94] approaches. Local hyperthermia can be used for a wide variety of medical interventions such as tumor ablation [Ste97, Ste98], treatment of heart arrhythmias [Lev95], local drug delivery with thermosensitive microcarriers [Kim93, Wei79] and control of gene therapy using heat-sensitive promoters [Mad98]. The objective of any thermal procedure is to provide adequate treatment of the entire target volume while sparing adjacent biological structures.

MRI is the only imaging technique that can provide both anatomical and quantitative thermometric information simultaneously.

Journal of WSCG, Vol.11, No.1., ISSN 1213-6972
WSCG'2003, February 3-7, 2003, Plzen, Czech Republic.

The main principle of MRI is based on the detection of magnetic properties of the protons contained in the water molecules of the body. Indeed, the water concentration of tissues varies from an organ to another or with its physiological state.

In order to estimate the quantity of protons in the tissues, the body is placed in a high-intensity magnetic field $\vec{B}_0$. Submitted to this magnetic field, the protons will become aligned along the direction of $\vec{B}_0$. This alignment is then perturbed by a short duration magnetic field $\vec{B}_1$ perpendicular to $\vec{B}_0$ and oscillating at a given frequency called the Larmor frequency (42.56 MHz/T for the proton). When $\vec{B}_1$ is suppressed, the protons return to their previous state in an oscillating movement. The movement of these dipoles induces a small magnetic field which is registered by the MRI antenna. This NMR (Nuclear Magnetic Resonance) signal is the sum S of all contributions of individual protons.

If $\vec{B}_0$ is homogeneous, all protons oscillate at the same frequency and it is therefore impossible to discriminate the protons in the 3D space. In order to provide imaging information it is necessary to superimpose a magnetic gradient $\vec{G}(x,y,z)$ to $\vec{B}_0$

following the three space coordinates. Thus each proton at a given set of coordinates *(x,y,z)* oscillates at a different frequency after $\vec{B}_1$ is released.

In the presence of $\vec{G}$, the signal *S* collected by the MRI antenna can be described by the following formula:

$$S(t) = \int_{-\infty}^{+\infty} M(x,y,z) e^{i\gamma(G_x x + G_y y + G_z z)t} dxdydz$$

where G_x, G_y and G_z are the values of $\vec{G}$ at the point *(x,y,z)*, γ is the gyromagnetic ratio and $\vec{M}(x,y,z)$ the magnetic density at the same point. This expression being a spatial Fourier transform, we can obtain directly $\vec{M}(x,y,z)$ by applying an inverse Fourier transform. In this work, we will focus on 2D slices. In this case, $\vec{M}(x,y)$ is represented by the complex number $Me^{i\varphi}$ where M is the magnitude and φ the phase. The corresponding graylevel of the anatomical image is proportional to M. φ is then used to construct a phase image (cf Figure 1).

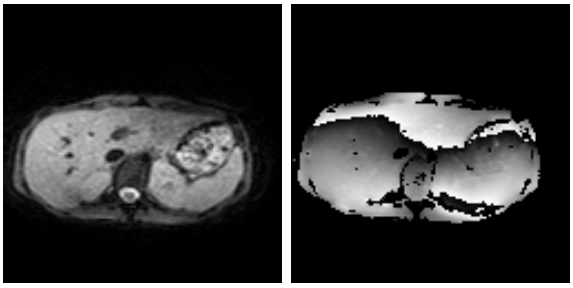

Figure 1: Magnitude and phase images of the abdomen

Under well-controlled conditions, a difference of phase is proportional to a difference of temperature. We can thus compute a temperature map by subtracting two subsequent phase images as shown in Figure 2.

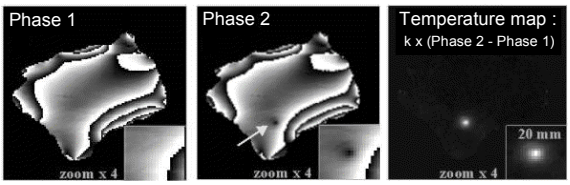

Figure 2: How to compute a temperature map

In this experiment, a well located area of an ex-vivo muscle sample was heated using a MR-compatible FUS device. Phase contrast due to local temperature change can be seen in the second phase image (arrow) and quantitative temperature map is obtained by subtracting the phase 2 image to the phase 1 image.

In order to monitor medical interventions such as tumor ablation by hyperthermia (necrosis of the tumor by a local temperature elevation), we need to have highly precise real-time temperature mapping technique (required precision should be in the range of 1°C for each pixel). The problem is that MRI suffers from three major sources of artefacts : noise generated by the MRI system itself, motions of the patient, and geometrical distortions. Since these artefacts are in part different in temperature mapping as compared to anatomical mapping, they need to be analyzed specifically.
The Figure 3 summarize the chain of process needed to obtain images.

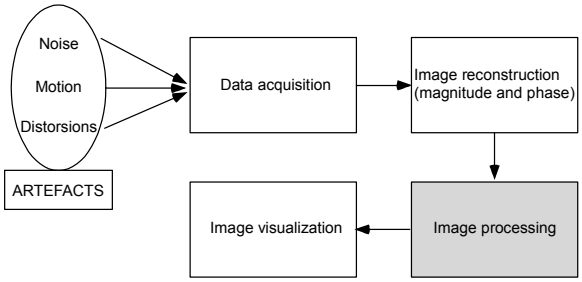

Figure 3: From acquisition to visualisation

Processing of an image must be done in the interval of time between two successive acquisitions (between 1s and 2s) to ensure real-time monitoring of temperature evolution.
In this paper, we present physical analysis of these sources of artefacts and we propose to attenuate them either by adapting the acquisition methods or by appropriate real-time processing.
Our test platform is a PC Duron 1GHz with 256 Mo of RAM.

2. NOISE REDUCTION

2.1 Noise modeling

It is well established that electronic noise is a Gaussian white noise [Ben62, Fin89]. The MRI system measures the real and imaginary components of the NMR signal. As these two measures are submitted to Gaussian white noise, the resulting noise will be a Rician stationary noise on the magnitude and the phase images (cf Figure 4).

Figure 4 presents the model of noise used in this study. To obtain the perturbation of a pixel $z = m.e^{i\varphi} = a + i.b$: each of the variables *a* and *b* are corrupted by a white noise having a Gaussian probability distribution using, for instance, the Box-Muller method [Box58].

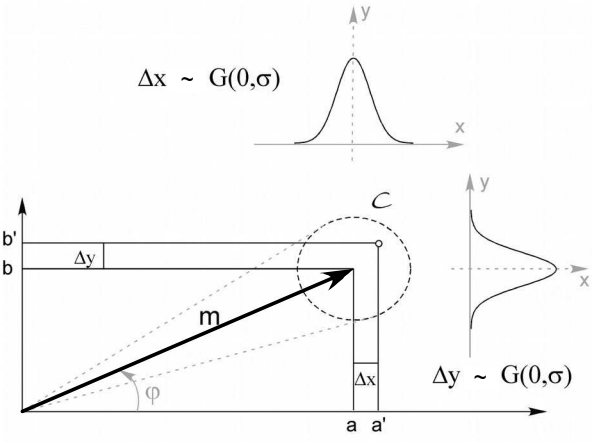

Figure 4: Rician noise

2.2 Noise Processing

The first two standard methods to attenuate noise effects are to change the data acquisition parameters. The first one (time-average) is to acquire n images and to average the value of each pixel in order to obtain one final image. As we compute temperature maps during a heating event, the phase images will be different from one to another. Therefore a temporal method is not useful. The second method (space-average) is to acquire image with a higher resolution and then to downsize the image by spatial smooth. This method does not apply in our case too, because it will increase the acquisition time for an image.

A classical method is to approximate the noise by a Gaussian noise. The correction is then done by applying a low-pass filter on the image. If this method provides generally a good result for the visualization of anatomic images, information will be lost in the phase image because phase is restrained to *[0,2π]*. Furthermore, the noise distribution in phase images is known to diverge from a near Gaussian distribution for images with a low SNR (Signal to Noise Ratio) [Gud95].

For temperature mapping, the previous approaches provide coarse results. We have shown in the 2.1 section that the noise in MR images follows a Rician distribution. Our method is to apply a low-pass filter not directly on the phase image but on real and on imaginary components and then to reconstruct the phase image. The results are displayed in the Figure 5 where the image (a) corresponds to an artificial phase image, (b) is the same image perturbed by an additive Gaussian white noise on the real and the imaginary components (SNR=10), (c) is the result obtained by filtering directly the phase image by a 2D Gaussian filter with a 5x5 mask and (d) by convoluting the real and the imaginary components by the same mask and reconstructing the phase image. It can be seen on this Figure that the last method leads to better results in terms of contrasts and of edge preservation with a similar filtering level.

As the MRI system provides real and imaginary components (as well as the magnitude and phase images), it is possible to filter out these two components directly. Then we reconstruct the phase image. If this method is more than two times slower than the direct filtering of the phase image, the convolution of an image by a 5x5 mask remains a fast operation (less than 0.09s for a 128x128 image on our test platform).

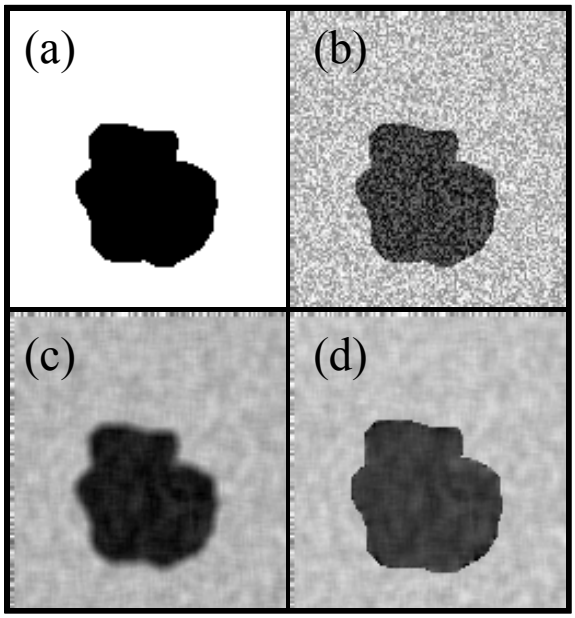

Figure 5: Noise reduction on a phase image

3. MOTION CORRECTION

The method used to obtain temperature mapping is based on the PRF (Proton Resonance Frequency) thermometry [Que00]. The temperature variation is proportional to a phase variation. The k[th] temperature mapping is computed using: $\Delta T_k = (\varphi_k - \varphi_0).C$, C being a constant and φ_0 and φ_k being the phase images at the instant 0 and the instant k, respectively.

When a movement occurs during the experiment (patient motion, respiration, cardiac activity), the phase difference induces erroneous temperature mapping. The sensitivity of this method has limited its application to the organs with little mobility or easily restrained like muscles [Haz02], breasts [Hyn01] and the prostate [Pet00].

3.1 Transformations

We will first describe the principal transformations used to make image registration.

Translation

The translation is a transformation that consists in moving objects in the image following a given direction vector *(A,B)* of space. The relation between the coordinate of a point *I(x,y)* in an image and its transformation *I'(x',y')* is :

$$\begin{pmatrix} x' \\ y' \\ 1 \end{pmatrix} = \begin{pmatrix} 1 & 0 & A \\ 0 & 1 & B \end{pmatrix} \cdot \begin{pmatrix} x \\ y \\ 1 \end{pmatrix}$$

Scale

The scale is a transformation that increases or decreases the size of an image by a factor *C* for the horizontal axis and a factor *D* for the vertical one.

$$\begin{pmatrix} x' \\ y' \end{pmatrix} = \begin{pmatrix} C & 0 \\ 0 & D \end{pmatrix} \cdot \begin{pmatrix} x \\ y \end{pmatrix}$$

Shearing

Shearing consists in stretching the image in a direction.

$$\begin{pmatrix} x' \\ y' \end{pmatrix} = \begin{pmatrix} 1 & E \\ F & 1 \end{pmatrix} \cdot \begin{pmatrix} x \\ y \end{pmatrix}$$

E and *F* being the horizontal and vertical coefficients of the shearing respectively.

Rotation

The rotation of an angle θ is a transformation that expresses *I'(x',y')* from *I(x,y)* with the matrix product :

$$\begin{pmatrix} x' \\ y' \end{pmatrix} = \begin{pmatrix} \cos\theta & \sin\theta \\ -\sin\theta & \cos\theta \end{pmatrix} \cdot \begin{pmatrix} x \\ y \end{pmatrix}$$

The composition of those transformations results from the product of the transformation matrices.

3.2 Motion correction techniques for thermometry

3.2.1 Physical approaches

Respiratory gating is a technique that allows reduction of respiration artefacts. The idea is to synchronize the acquisition of the images to a stable period of the respiratory cycle, usually at the end of expiration [Mor02] (see Figure 7). Real time evolution of the respiration can be obtained (on the MRI console) by using a pressure transducer positioned on the abdomen. The major drawback of this method is that the temporal resolution depends on the respiration frequency. Moreover, artefacts due to irregular and/or deep respiration movements induce erroneous temperature mapping.

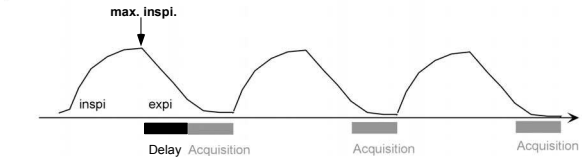

Figure 7: respiratory gating

The echo navigator [Zwa01] uses an approach that consists of acquiring one line of Fourier space containing the origin and applying an inverse Fourier transformation in order to get the profile of the object. This technique can only correct translation movements.

Radial acquisition [Sch99] is an MRI acquisition method of the images with little sensitivity to motion artefacts. It consists in making a radial acquisition of each line of Fourier space containing the origin. Each line is an echo navigator itself and motion correction is performed on each echo, prior to the inverse Fourier transform. This technique gives good results for correcting the respiration artefact but only if the respiration is neither too ample nor too fast.

3.2.2 Computational approaches

Another approach consists in using the reference images to detect in real-time the movements on the anatomic images to correct the erroneous temperature map. The objective is to relate the coordinate of each part of tissue in of the image we want to register with the corresponding tissue in the reference image.

Fourier-based image registration algorithm

The Fourier Transform has already been introduced to register images that are misaligned due to translation, rotation and scale [Cas87]. Registration problems involving pure translation can be recovered by applying the Fourier Transform and using phase correlation [Kug75]. A log-polar transformation is applied to the magnitude spectrum and the rotation and scale is recovered by using phase correlation in the log-polar space [Red96, Wol00]. This method exploits the fact that by operating on the magnitude spectrum of an image, the translational differences are avoided since the magnitude spectrum of an image and its translated counterpart is identical; only their phase spectrum is different. Furthermore, the log-polar transformation causes rotation and scale to be recognized as translation, whereby phase correlation can be applied to recover the rotation angle and scale factor between the pair of input

images. Results obtained are very satisfying for the announced assumptions. This technique doesn't require long time computation as it only needs six Fourier Transformation, one log-polar conversion, one rotation and one scale.

Square root optimization

This technique is used in the software SPM [SPM] designed to register on functional MR images. The objective of this method is to determine a set of parameters for which some function of the parameters is minimized (or maximized). One of the simplest cases is determining the optimum parameters for a model in order to minimize the sum of squared differences between the model and a set of real world data (χ^2). Usually there are many parameters in the model and it is not possible to exhaustively search through the whole parameter space. This image registration approach is essentially an optimization which tries to get a minimal χ^2. The optimized parameters are the ones which describe the spatial transformation. The algorithm of choice [Fri95] is similar to Gauss-Newton optimization: $d_i(p)$ is the function describing the difference between the image to be registrated and the reference image at the voxel i where the vector of model parameters have values p. For each voxel i, a first approximation of Taylor's Theorem can be used to estimate the value that this difference will take if the parameters p are increased by t :

$$d_i(p+t) = d_i(p) + t_1 \frac{\partial d_i(p)}{\partial p_1} + t_2 \frac{\partial d_i(p)}{\partial p_2} + \ldots$$

From this, a set of simultaneous equations can be set up to estimate the values that t should take to minimize $\sum_i d_i(p+t)^2$:

$$\begin{pmatrix} -\frac{\partial d_1(p)}{\partial p_1} & -\frac{\partial d_1(p)}{\partial p_2} & . & . & . \\ -\frac{\partial d_2(p)}{\partial p_1} & -\frac{\partial d_2(p)}{\partial p_2} & . & . & . \\ . & . & . & & \\ . & . & & . & \\ . & . & & & \end{pmatrix} \begin{pmatrix} t_1 \\ t_2 \\ . \\ . \\ . \end{pmatrix} \approx \begin{pmatrix} d_1(p) \\ d_2(p) \\ . \\ . \\ . \end{pmatrix}$$

From this we can derive an iterative scheme for improving the parameter estimates. For the iteration n, the parameters p are updated as:

$$p^{n+1} = p^n + \left(A^T A\right)^{-1} A^T b$$

where

$$A = \begin{pmatrix} -\frac{\partial d_1(p)}{\partial p_1} & -\frac{\partial d_1(p)}{\partial p_2} & . & . & . \\ -\frac{\partial d_2(p)}{\partial p_1} & -\frac{\partial d_2(p)}{\partial p_2} & . & . & . \\ . & . & . & & \\ . & . & & . & \\ . & . & & & \end{pmatrix} \text{ and } b = \begin{pmatrix} d_1(p) \\ d_2(p) \\ . \\ . \\ . \end{pmatrix}$$

"Block-matching" algorithm

This technique is used in the compression of videos in the MPEG format. The image to be registered (I) is divided in blocks. If $x0$ and $y0$ are the coordinate of the origin of one of these blocks, we want to compute, in the reference image (I_{ref}), the translation (Δx, Δy) that minimize:

$$\sum_{0 \le x,y} \left| I(x_0 + x, y_0 + y) - I_{ref}(x_0 + x + \Delta x, y_0 + y + \Delta y) \right|$$

This technique is less restrictive than the others as we don't have to fix a transformation between the image to be register and the reference image.

3.2.3 Application to real-time thermometry

Even if physical approaches are necessary to optimize the acquisition procedure, they do not guarantee that temperature maps will be stable enough to obtain a reliable MRI thermometry. As a consequence, additional image processing is required to improve stability of the method.

The inconvenience of the square root optimization is that there is no guarantee that the best global solution will be reached, since the algorithm can get caught in a local minimum. To reduce this problem, the starting estimates for p should be as close as possible to the optimum solution. Similarly, the "Block-matching" registration gives good results only for small motions. Fourier-based methods do not search in parameter space; therefore we do not have this restriction of efficiency. On the other hand square root optimization is less restrictive than the Fourier-based image registration as it is possible to determine transformations defined with a set of parameters. The more permissive method is the "Block-

matching" algorithm because there is no limitation with the transformation that can be applied to the original image.

Thus, the choice of the method depends on the part of the body observed. Different possible applications are summarized in Table 1.

Organ	Transfor-mation	More efficient algorithm	Computation time for 128x128 images
Brain, neck	translation + rotation + scale	Fourier-based algorithm	0.42s
		Square root optimization (9 parameters)	0.54s
Kidney, muscles, prostate, uterus	translation + rotation + scale + shearing	Square root optimization (12 parameters)	0.63s
Liver, breast	Complex	"Block-matching" algorithm	0.19s

Table 1 : computing time of the different methods

4. GEOMETRIC DISTORTIONS

4.1 Modeling of the distortion

The MR-magnet localizes the source and the intensity of the signal with the measured proton resonance frequency (see section 1). The presence of local inhomogeneities of the magnetic field in the IRM (susceptibility variations) generates errors in this localization and induces geometric distortions in the MR image. Those distortions are amplified by the specificity of the acquisition parameters required to perform real-time thermometry. Those distortions affect both magnitude and phase images and may produce erroneous anatomic images and temperature mapping.

Geometric distortions induce a translation of the pixels of the image in a main direction of the space (so called "Phase encoding direction"). The amplitude of the translation for a given pixel is proportional to the magnetic field at this point. All images presented are obtained using a test phantom composed of a water filled bucket in which seven 2cm diameter tubes were placed. The tubes contained a gadolinium DTPA solution at different concentrations in order to produce different susceptibility artefacts and contrast.

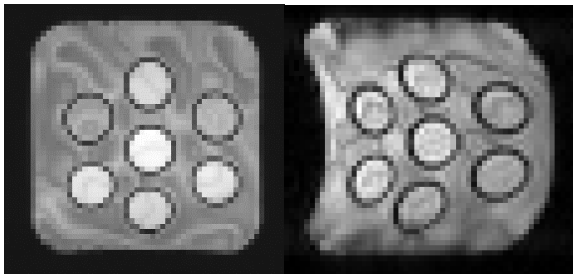

Figure 8: optimal parameters and distorted image

Figure 8 displays an image acquired with optimal parameters and the typical distorted image obtained with real-time thermometry parameters.

4.2 Image processing

Classical method

The solution proposed by the Bristol Oncology Centre [BOC] is to consider that patient specific distortions are reduced to an insignificant level by careful choice of examination protocol. It then remains to calibrate and to correct for system dependent geometric warp of images. A MR phantom was constructed composing of a series of fluid filled spheres on a rectangular grid. Images of this test sample are obtained with series of different protocols with the frequency and phase encode directions swapped and covering the whole useful imaging volume. Analysis of the data produced allows separation of the distortion due to main field and gradient related effects. A look up table of geometric correction vectors is produced that may be applied both to anatomic and phase image. This method is easy to implement. The major drawback is that the distortion in the subject is not computed but is deduced from the distortion outside the subject.

Our method

Another approach consists in computing the magnetic field on all the pixels of the image. From this, we'll be able to calculate precisely the translation of the pixels of the image. We can have a good estimation of the magnetic field in the IRM by making the difference of two phase images acquired with different acquisition parameters: if we call φ_1 the phase image when there is no perturbation and φ_2 the phase image when there is a perturbation, then the perturbation of the magnetic field is given by $(\varphi_2 - \varphi_1).C$, C being a constant.

Phase values are restricted in $[0,2\pi]$. The main difficulty is to unwrap the phase and to interpolate the values in the pixels where signal interest is poor. Typical results obtained on our test phantom are presented on Figure 9.

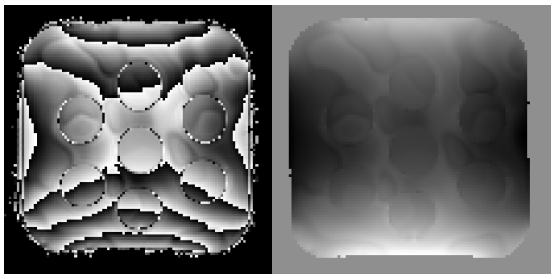

Figure 9: initial phase image and unwrapped and interpolated phase image

The resulting magnetic field is shown on Figure 10.

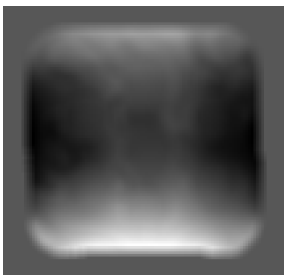

Figure 10: correction matrix of distortion derived from $(\varphi_2 - \varphi_1).C$

The correction of the geometric distortions with this method gives the following result displayed on Figure 11.

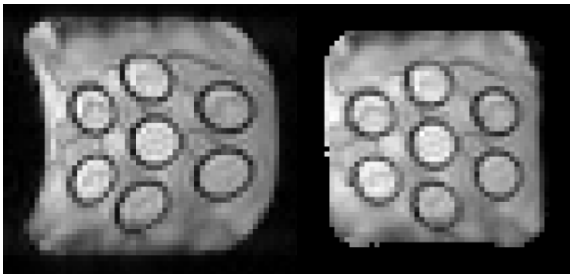

Figure 11: geometric distortion correction

The main advantage of this technique is that we can compute a correction matrix before launching the acquisition of temperature maps, and correct each image acquired during the experiment with the same correction matrix, assuming a stationary perturbation over the experiment.

This method can be easily applied to the thermometry because the influence of the phase variation induced by heating is too little to provoke errors in the correction. This method is suitable for immobile objects and has to be tested in the presence of motion (work in progress). The time computation of this method on our test platform is around 0.20s.

5. RESULTS

To summarize, the image processing block of the Figure 3 can be decomposed as in Figure 12 by a chain of treatment.

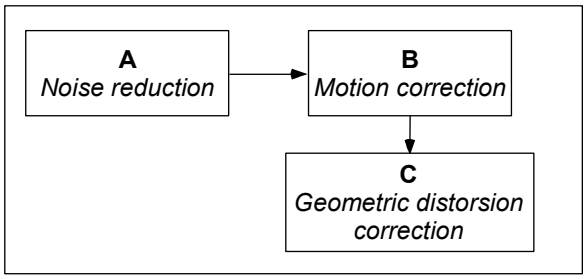

Figure 12: image processing block

On our test platform, the noise reduction process computational time for a 128x128 image is 0.40s (two times 0.18s for the treatment of the real component and the imaginary component of the image and 0.02s for reconstructing the phase image). The range of time for the motion correction is between 0.19s and 0.63s depending on the organ and the method considered (see Table 1). Finally the geometric distortion correction takes 0.20s. Therefore the total computing time is between 0.79s and 1.23s. As the acquisition time between two images is in the range of 1s to 2s, we can achieve real-time processing.

6. CONCLUSION AND FURTHER WORK

In this paper, the three major sources of artefacts in MR images have been presented. Algorithms, based on the physical description of these artefacts, and adapted to the real-time temperature mapping, were also presented. Although these algorithms are efficient, we still have to combine them in order to optimize their action or to avoid side effects. Furthermore, MRI system can provide us with 3D images (either directly or by stacking 2D images). We plan to adapt our algorithms to the 3D case, but the accuracy of 3D temperature mapping has still to be tested.

7. ACKNOWLEDGEMENTS

The authors would like to thank Rares Salomir for his help and the physiology / therapy team of the RMSB.

8. REFERENCES

[Ben62] Bennett, W.R., Electrical Noise. McGraw Hill, New-York, 1962

[BOC] Open MR Scanner, Level A, Bristol Oncology Centre, Horfield Road, Bristol, BS2 8ED http://www.bris.ac.uk/Depts/Oncology/BOC/

[Box58] Box, G.E.P., M.E. Muller 1958; A note on the generation of random normal deviates, Annals Math. Stat, V. 29, pp. 610-611

[Cas87] E. De Castro and C. Morandi. Registration of translated and rotated images using finite Fourier

transforms. IEEE Trans. Pattern Analysis and Machine Intelligence, (3):700-703, September 1987

[Cli94] Cline H.E., Hynynen K., Hardy C.J., et al. MR temperature mapping of focused ultrasound surgery. Magn Res. Med. 1994;31:628-636.

[Fin89] Fink, D.G., Christiansen, D., Electronic engineer's handbook. 3rd edition.4.46-4.49, 1989

[Fri95] Friston K.J., Ashburner J, Frith C.D., Poline J-B., Heather J.D. and Frackowiak R.S.J. Spatial registration and normalisation of images. Human Brain Mapping. 2:165-189. 1995.

[Ger98] Germer C., Isbert C.M., Albrecht D. et al. Laser-induced thermotherapy for the treatment of liver metastasis. Correlation of gadolinium-DTPA-enhanced MRI with histomorphologic findings to determine criteria for follow-up monitoring. Surg. Endosc. 1998;12:1317-1325.

[Gud95] Gudjartsson H., Patz S., The Rician Distribution of Noisy MRI Data. Magnetic Resonance in Medicine 1995:34;910-914.

[Haz02] Hazle JD, Stafford RJ, Price RE. Magnetic resonance imaging-guided focused ultrasound thermal therapy in experimental animal models : correlation of ablation volumes with pathology in rabbit muscle and VX2 tumors. J Magn Res Imaging. 2002; 15 : 185-194.

[Hyn01] Hynynen K, Pomeroy O, Smith DN, Huber PE, McDannold NJ, Kettenbach J, Baum J, Singer S, Jolesz FA. MR imaging-guided focused ultrasound surgery of fibroadenomas in the breast : a feasibility study. Radiology. 2001; 219 : 176-85.

[Kim93] Kim S. Liposomes as carriers of cancer chemotherapy: current status and future prospects. Drugs 1993;46:618-638.

[Kug75] Kuglin C.D. and Hines D.C.. The phase correlation image aligment method. Proc. Int. Conf. On Cybernetics and Society, pages 163-165, 1975.

[Lev95] Levy S. Biophysical basis and cardiac lesions caused by different techniques of cardiac arrhythmia ablation. Arch. Mal. Coeur Vaiss. 1995;88:1465-1469.

[Mad98] Madio D.P., van Gelderen P., DesPres D., et al. On the feasibility of MRI-guided focused ultrasound for local induction of gene expression. J. Magn. Res. Imaging 1998;8:101-104

[Mor02] Moricawa S, Inubushi T, Kurumi Y, Naka S, Seshan V, Tsukamoto T. Feasibility of simple respiratory triggering in MR-guided interventional procedures for liver tumors under general anesthesia. ISMRM, 10th Annual Meeting, Hawaï. 2002.

[Pet00] Peters RD, Chan E, Trachtenberg J, Jothy S, Kapusta L, Kucharczyk W, Henkelman RM. Magnetic resonance thermometry for predicting thermal damage: an application of interstitial laser coagulation in an in vivo canine prostate model. Magn Res Med. 2000; 44 : 873-83.

[Que00] Bruno Quesson, Jacco A. de Swart, Chrit T.W. Moonen, Magnetic Resonance Temperature Imaging for Guidance of Thermotherapy. Journal of Magnetic Resonance Imaging, 2000;12:523-533.

[Red96] B.S. Reddy and B.N. Chatterji. An fft-based technique for translation, rotation, and scale-invariant image registration. IEEE Trans. Pattern Analyses and Machine Intelligence, 5(8):1266-1270, August 1996

[Sam92] Samulski T.V., MacFall J., Zhang Y., Grant W., Charles C., Non-invasive thermometry using magnetic resonance diffusion imaging: potential for application in hyperthermic oncology. Int. J. Hyperthermia 1992;8:819-829

[Sch95] Schwarzmaier H.J., Kahn T., Magnetic resonance imaging of microwave induced tissue heating. Magn. Res. Med. 1993;33:729-731.

[Sch99] Schaffter T., Rasche V., Carlsen I.C**.** Motion compensated projection reconstruction. Magn Res Med 1999 May;41(5):954-63.

[Sch01] Schaeffter T, Weiss S, Rasche V. Radial MRI – a motion insensitive temperature mapping method. ISMRM, 10th Annual Meeting, Glasgow. 2001

[SPM] http://www.fil.ion.ucl.ac.uk/spm/

[Ste97] Steiner P., Botnar R., Goldberg S.N., Gazelle G.S., Debatin J.F. Monitoring of radio frequency tissue ablation in an interventional magnetic resonance environment. Preliminary ex-vivo and in-vivo results. Invest. Radio. 1997;32:671-678

[Ste98] Steiner P., Botnar R., Dubno B. et al. Radio-frequency induced thermoablation: monitoring with T1-weighted and proton frequency shift MR imaging in an interventional 0.5-T environment. Radiology 1998;206:803-810.

[Vit97] Vitkin I.A., Moriarty J.A., Peters R.D. et al. Magnetic resonance imaging of temperature changes during intersticial microwave heating : a phantom study. Med. Phys. 1997;24:269-277.

[Wei79] Weinstein J.N., Magin R.L., Yatvin M.B., Zaharko D.S. Liposomes and local hyperthermia: selective delivery of methotrexate to heated tumors. Science 1979;204:188-191.

[Wlo98] Wlodarczyk W., Boroschewski R., Hentschel M., et al. Three-dimensional monitoring of small temperature changes for therapeutic hyperthermia using MR. J. Magn. Res. Imaging 1997;7:918-928

[Wol00] George Wolberg, Siavash Zokai, Robust Image Registration Using Log-Polar Transform. Department of computer Science, City College of New York.2000.

[Zwa01] Jacco A. de Zwart, Frédéric C. Vimeux, Jean Palussière, Rares Salomir, Bruno Quesson, Christophe Delalande, and Chrit T.W. Moonen, On-Line Correction and Visualiszation of Motion During MRI-Controlled Hyperthermia. Magnetic Resonance in Medicine. 2001; 45:128-137.